International Journal of General Medicine

Dovepress
Taylor & Francis Group

Open Access Full Text Article

ORIGINAL RESEARCH

Identification the Tumor Mechanics-Related Biomarkers in Gastric Cancer Patients Based on Bioinformatics and Machine Learning

Minzhi Sun[1,2], Qing Liu[3], Aman Xu[1]

[1]Department of General Surgery, The First Affiliated Hospital of Anhui Medical University, Hefei, People's Republic of China; [2]Anhui Public Health Clinical Center, Hefei, People's Republic of China; [3]Department of Gynecology and Obstetrics, The Second Affiliated Hospital of Anhui Medical University, Hefei, People's Republic of China

Correspondence: Aman Xu, Department of General Surgery, The First Affiliated Hospital of Anhui Medical University, Hefei, 230022, People's Republic of China, Email xuaman@ahmu.edu.cn

Background: Gastric cancer (GC) remains a major cause of cancer related mortality worldwide. Tumor mechanics, reflecting the physical and mechanical properties that influence tumor cell behavior and the tumor microenvironment (TME), play important roles in cancer progression. However, the prognostic relevance of tumor mechanics-related genes (MRGs) in GC remains unclear.

Methods: GC datasets from TCGA and GEO were analyzed to identify differentially expressed genes (DEGs). WGCNA was conducted to identify MRGs-related modules. Univariate Cox regression and three machine learning algorithms were applied to screen prognostic genes and construct a prognostic model. Pan-cancer analysis, immune infiltration, tumor mutation burden (TMB), immunophenotypic score (IPS), and somatic mutation analyses were performed to explore TME characteristics. Additionally, drug sensitivity and ceRNA network analyses were conducted. Finally, the prognostic genes were verified using RT-PCR.

Results: Eight mechanics-related genes (SERPINE1, CYP1B1, LOX, HEYL, VCAN, IGFBP7, TWIST2, and ATP1B2) were identified through integrated computational analysis. The resulting model demonstrated prognostic potential for 2-, 3-, and 5-year survival prediction. High-risk patients exhibited increased immunosuppressive infiltration compared with low-risk patients. Drug sensitivity analysis revealed significant differences in therapeutic responses across risk groups. Finally, the differential expression of several prognostic genes was preliminarily confirmed by RT-PCR in limited tissue samples.

Conclusion: This study identifies eight tumor mechanics-related genes as prognostic biomarkers for GC through comprehensive bioinformatic analyses. These findings may provide preliminary insights into prognostic assessment and targeted therapy for GC, although further validation with larger sample sizes is required to substantiate their clinical applicability.

Keywords: gastric cancer, tumor mechanics-related genes, prognostic model, prognostic genes, tumor immune microenvironment

Introduction

Gastric cancer (GC) is the fifth most common malignant cancer worldwide, characterized by high aggressiveness and a strong tendency for metastasis.[1–3] Despite advances in the diagnosis and treatment of GC in recent years, the long-term survival of patients remains unsatisfactory.[4,5] Meanwhile, the progression of GC is a complex biological process influenced by the coordinated interactions among multiple cell types and signaling pathways.[6–8] The tumor microenvironment (TME) is composed of tumor cells, endothelial cells, fibroblasts, and a variety of immune cells. It plays a crucial role in the progression of GC by forming a complex regulatory signaling network.[9,10]

Tumor mechanics focuses on the physical and mechanical properties that regulate the behavior of tumor cells and their surrounding microenvironment. Studies have shown that tumor cells reside in a complex microenvironment composed of various biomechanical factors, such as extracellular matrix (ECM) rigidity, interstitial fluid pressure, and mechanical stress.[11] Recent studies have confirmed that the physical properties of tumor tissue and the TME jointly regulate tumor initiation, development, metastasis, and therapeutic sensitivity.[12] Compared with normal tissues, physical

Received: 31 July 2025
Accepted: 8 December 2025
Published: 18 December 2025

characteristics such as tumor stiffness, elasticity, fluidity, and the composition of surrounding structures exhibit significant abnormalities that may promote malignant progression.[13] In addition, the rapid proliferation of tumor cells exerts mechanical forces on adjacent normal tissues, forcing the local microenvironment to undergo continuous adaptation and ultimately leading to profound alterations in the TME.[14,15] Notably, the TME regulates tumor cell behavior by activating mechanical signaling pathways such as integrins, Piezo1/2, and YAP/TAZ.[16] These pathways not only transmit biochemical cues but also influence immune cell infiltration and clinical treatment outcomes.[17,18] For example, in GC, Piezo1 can directly promote tumor progression by activating the PI3K/AKT/mTOR signaling pathway, and indirectly facilitate tumor growth by enhancing the infiltration of immunosuppressive cells while reducing anti-tumor immune cells, thereby creating an immunosuppressive microenvironment.[19,20] Recently, Zhang et al reported a set of mechanics-related genes associated with biomechanical properties such as ECM composition, cell proliferation, and adhesion. This gene set reflects biological processes through which biomechanical forces influence tumor progression and therapeutic responses.[21] Therefore, we applied this 79-gene mechanical signature to GC to investigate its prognostic significance. Exploring prognostic genes from the perspective of tumor mechanics may provide novel biomarkers for mechanical diagnosis, risk stratification, and mechanobiological therapy in GC.

In this study, we integrated transcriptomic and clinical data from TCGA and GEO to identify differentially expressed tumor mechanics-related genes in GC and to develop and validate a prognostic model. Additionally, we explored the association of the risk signature with the TME and drug sensitivity. Finally, the expression levels of the prognostic genes were further validated by RT-PCR. This study may provide new insights for early screening, precise treatment, and prognosis prediction of GC.

Materials and Methods

Data Acquisition and Pre-Processing

Transcriptome data of GC were downloaded from The Cancer Genome Atlas (TCGA, https://www.cancer.gov/tcga), comprising 368 GC samples and 33 normal samples. In addition, the datasets GSE84437 (431 GC samples), GSE66229 (300 GC samples and 100 normal samples), and GSE54129 (111 GC samples and 21 normal samples) were downloaded from the Gene Expression Omnibus (GEO, https://www.ncbi.nlm.nih.gov/geo). To avoid the impact of non–tumor-related death and to minimize statistical bias, subsequent analyses included only patients with complete clinical survival data, excluding those with an overall survival (OS) shorter than 30 days.[22,23] Furthermore, mechanics-related genes (MRGs) were obtained from previously published literature (Table S1).[21]

Differential Expression Analysis

We first performed differential expression analysis on the TCGA dataset using the R package limma (v 3.62.1). Genes with P.adj < 0.05 and $|\log2FC| > 0.5$ were considered differentially expressed genes (DEGs).

Weighted Gene Co-Expression Network Analysis

To expand the potential genes associated with MRG in GC, we applied the weighted gene co-expression network analysis (WGCNA) and identified the significant gene modules with MRG. Initially, single-sample gene set enrichment analysis (ssGSEA) scores (MRG scores) were calculated for each sample.[24] Next, to construct a scale-free co-expression network, a series of soft-thresholding powers (β) were evaluated, and the optimal value was selected based on the scale-free topology criterion ($R^2 > 0.85$) together with an assessment of mean connectivity. During this procedure, the scale-free topology fit curve showed that $\beta = 5$ was the first power at which the R^2 value approached 0.9, satisfying the predefined criterion and aligning with WGCNA's recommended strategy for parameter selection. Accordingly, $\beta = 5$ was chosen as the soft-thresholding power. The topological overlap matrix (TOM) was then calculated to quantify network interconnectedness, followed by hierarchical clustering using average linkage and dynamic tree cutting (minimum module size = 50 genes) to identify robust modules. Finally, the gene module most significantly correlated with the MRG score was identified as the key gene module (WGCNA-MRGs) for further analysis.

Screening and Functional Enrichment Analysis of GC Mechanics-Related Genes

We intersected the DEGs with WGCNA-MRGs to obtain tumor mechanics-related genes (T-MRGs). To explore the biological processes and regulatory pathways associated with the T-MRGs, we performed Gene Ontology (GO) enrichment and Kyoto Encyclopedia of Genes and Genomes (KEGG) pathway analyses using the R package clusterProfiler (v 4.12.6)[25,26.] The protein-protein interaction (PPI) network of tumor mechanics-related genes was obtained from the STRING website (interaction score > 0.15; https://string-db.org/).[27]

Construction and Evaluation of Prognostic Models

Candidate MRGs significantly associated with patient survival were first screened using univariate Cox regression analysis, and genes with $p < 0.05$ were retained. Subsequently, the TCGA cohort was randomly divided into training and testing sets at a 1:1 ratio, and further filtering was performed in the training set. A hierarchical machine learning pipeline was subsequently applied to refine the Cox-filtered gene set. First, XGBoost was used to rank feature importance based on tree-based contribution scores. The top 40 ranked genes identified by XGBoost were subsequently input into SVM to eliminate redundant predictors and retain the most informative subset. The SVM analysis was implemented using the caret R package with function rfe. A 10-fold cross-validation procedure (method = "cv", number = 10) was employed to select the optimal feature subset. Finally, to further optimize feature selection, LASSO Cox regression was performed, and the optimal penalty parameter was determined via 10-fold cross-validation (lambda.min = 0.03303032). A multivariate Cox regression model was constructed using the LASSO-selected genes, and a risk score was calculated for each patient. Patients were then stratified into high- and low-risk groups based on the median risk score. The receiver operating characteristic (ROC) curve was plotted using the R package timeROC (v 1.18.5) to assess the model's discriminative ability. Meanwhile, Kaplan-Meier (KM) survival analysis was performed to compare survival differences between risk groups and clinical subgroups. Additionally, to evaluate the relationship between prognostic risk scores and clinical features, the Wilcoxon rank-sum test was applied. To further visualize the contribution of each variable and its impact on patient survival, a nomogram was constructed using the R package regplot (v 1.1). Calibration curves were subsequently utilized to evaluate the accuracy and reliability of the nomogram.

Pan-Cancer Analysis and Functional Enrichment Analysis

To investigate potential biomarkers across various cancer types, the Gene Set Cancer Analysis (GSCA) database (http://bioinfo.life.hust.edu.cn/GSCA/) was used to analyze the expression patterns of the identified prognostic genes in other cancers.[28] First, the R package DESeq2 (v 1.44.0) was applied to assess gene expression differences between the high- and low-risk groups. Subsequently, to further explore the potential functional characteristics of the DEGs, gene set enrichment analysis (GSEA) was performed using the R package clusterProfiler (v 4.12.6).[29] Functional annotation was conducted based on gene sets obtained from the Molecular Signatures Database (MSigDB; https://www.gsea-msigdb.org/gsea/msigdb).[30] Enrichment results with $p < 0.05$ and $|NES| > 1$ were considered statistically significant.

Immune Infiltration Analysis Between Risk Groups

To compare immune and stromal components between the two risk groups, the ESTIMATE algorithm (R package ESTIMATE, v 0.99.0) was used with method = "estimate" and default parameters.[31] Infiltration scores for 28 immune cell types were calculated using ssGSEA (v 1.52.3) with default settings (minSize = 1, maxSize = Inf, alpha = 0.25, normalize = TRUE). Here, alpha = 0.25 represents the recommended weighting exponent used to moderate the impact of highly expressed genes, while normalization ensures comparability across samples. Additionally, the MCP-counter algorithm (R package MCP-counter, v 0.99.0) was used to quantify the infiltration of eight immune cell types and two stromal cell types (endothelial cells and fibroblasts).[32]

Anti-Cancer Immune Cycle, Immunophenotypic and Somatic Mutation Analyses

To examine differences in the activity of the seven steps of the cancer immunity cycle between the two risk groups, activity scores were obtained from the Tracking Tumor Immunophenotype (TIP) platform (https://biocc.hrbmu.edu.cn/

TIP/).[33] Additionally, immune phenotypes related to GC were obtained from The Cancer Immunome Atlas (TCIA; https://tcia.at/home) to evaluate the potential responsiveness to immunotherapy. Finally, somatic mutation data from GC samples were obtained using the R package TCGAmutations (v 0.4.0) and visualized using maftools (v 2.20.0).

Drug Sensitivity Analysis and Competing Endogenous RNA (ceRNA) Analysis

To assess drug sensitivity of GC samples, we used the Genomics of Drug Sensitivity in Cancer (GDSC; https://www.cancerrxgene.org/) database and the R package pRRophetic (v 0.5). Furthermore, to elucidate the regulatory mechanisms underlying prognostic genes, we identified potential miRNAs using miRanda (http://www.microrna.org/), MicroCosm (https://tools4mirs.org/software/mirna_databases/microcosm-targets/), and TargetScan (https://www.targetscan.org/vert_80/). Additionally, lncRNAs with interaction scores greater than 2 were obtained from the StarBase database (https://rnasysu.com/encori/). Finally, the lncRNA-miRNA-mRNA regulatory networks were visualized using the R package ggalluvial (v 0.12.5).

RT-PCR

Six GC tissues and six adjacent non-tumor tissues were collected from The First Affiliated Hospital of Anhui Medical University. This study was conducted in accordance with the Declaration of Helsinki and was approved by the Ethics Committee of The First Affiliated Hospital of Anhui Medical University (approval number: PJ-YX2025-043) on July 1, 2025 (Supplementary Documents 1 and 2). At the same time, informed consent was obtained from all subjects involved in the study. Total RNA was extracted from GC tissues and tumor-adjacent tissues using the TRIzol (Tiangen, China). Subsequently, cDNA synthesis was performed using the Hifair® III 1st strand cDNA synthesis supermix, according to the manufacturer's protocol. RT-PCR amplification was conducted to detect the expression of identified prognostic genes. The primer sequences used are listed in Table 1. Gene expression relative to β-actin was determined using the $2^{-\Delta\Delta Ct}$ method.

Statistical Analysis

All statistical analyses and plots were conducted using R software (v 4.4.1) and GraphPad Prism (v 10.1.2). For comparisons between groups, the Wilcoxon rank-sum test was used for non-normally distributed data, whereas the Student's *t*-test was applied for normally distributed data. Correlation analysis was assessed using Spearman's method. For analyses involving large-scale multiple testing, including differential expression analysis, functional enrichment analysis, and immune scores between high- and low-risk groups, P values were adjusted using the Benjamini–Hochberg

Table 1 The Primers Used in This Study

Primer Names	Sequence
Homo-EAF1-F	ACAAACGGCCTTACCAGAAAG
Homo-EAF1-R	AATGCTGCTACTGAGTTTTTCCA
Homo-HMGN4-F	GATCAGCTCGGTTGTCTGCTA
Homo-HMGN4-R	GCAGGGTTGTTCCCATCCTT
Homo-KRT10-F	TCCTACTTGGACAAAGTTCGGG
Homo-KRT10-R	CCCCTGATGTGAGTTGCCA
Homo-MAPRE1-F	AAGCTAGAACACGAGTACATCCA
Homo-MAPRE1-R	AGTTTCTTGACCTTGTCTGGC
Homo-NUCKS1-F	GGCCTGTCAGAAATAGGAAGGT
Homo-NUCKS1-R	TTTAGCTTCTCGGGGAGATGAT
Homo-VARS-F	TACGCCGACACGGAGTTAATA
Homo-VARS-R	TCTAGGACGTATCGGAAAGGC
Homo-ACTIN-F	CATGTACGTTGCTATCCAGGC
Homo-ACTIN-R	CTCCTTAATGTCACGCACGAT

false discovery rate (FDR). For analyses with a limited number of pre-specified comparisons (eg, risk scores across limited clinical subgroups), unadjusted two-sided P values were reported. Statistical significance was defined as $P < 0.05$.

Results

Identification and Functional Analysis of Tumor Mechanics-Related Genes in GC

A total of 3636 DEGs (1770 upregulated genes and 1866 downregulated genes) were identified from the TCGA dataset (Figure 1A). To evaluate the enrichment of MRGs in each GC patient and normal sample, we performed ssGSEA. The ssGSEA analysis revealed a significant difference between the GC and control groups, providing a basis for subsequent analyses (Figure 1B). Initially, the "goodSamplesGenes" function was employed to remove outliers and unqualified samples, and sample dendrogram and heatmap were constructed (Figure S1A). To construct the gene co-expression network, the optimal soft-thresholding power was set to 5 ($R^2 \approx 0.9$, minimum module size = 50), resulting in the identification of 15 distinct gene modules (Figure 1C–E). Subsequently, the correlations between gene modules and clinical traits were assessed to identify key modules. As shown in Figure 1F, the purple and cyan modules exhibited the strongest correlations with MRG scores. These two modules collectively contained 724 genes, which were subsequently defined as the WGCNA-MRGs (Figure 1G and H).

By intersecting the DEGs with WGCNA-MRGs, 248 T-MRGs were identified (Figure 1I). To explore their potential biological roles, functional enrichment analyses were performed. Functional enrichment analysis revealed that these genes were significantly enriched in GO terms, including external encapsulating structure organization, extracellular matrix structural constituent, and collagen-containing extracellular matrix (Figure S1B). Moreover, several signaling pathways, including the PI3K-Akt signaling pathway, protein digestion and absorption, and ECM-receptor interaction, were also significantly enriched (Figure 1J). From the 248 genes, a PPI network was generated, containing 246 nodes and 7,288 edges (Figure S1C).

Machine Learning-Based Identification of Prognostic Genes and Risk Model Construction in GC

To identify prognostic genes, three machine learning approaches were applied to the 248 T-MRGs. First, univariate Cox regression was utilized to filter genes, resulting in the identification of 189 genes with $p < 0.05$. The 20 genes exhibiting the strongest associations were highlighted in Figure 2A. Subsequently, the top 40 genes were determined using the XGBoost algorithm (Figure 2B). Based on the results from the XGBoost algorithm, the SVM algorithm further identified 37 genes (Figure 2C). Finally, a novel prognostic signature was constructed through LASSO regression analysis, leading to the identification of 8 genes, SERPINE1, CYP1B1, LOX, HEYL, VCAN, IGFBP7, TWIST2, and ATP1B2 (Figure 2D).

Using multivariate Cox regression analysis, a prognostic model was constructed, with the regression coefficients for each gene detailed in Table 2. The formula for the prognostic model is as follows: RiskScore = (0.494995 × expression value of SERPINE1) + (0.154756 × expression value of CYP1B1) + (0.298706 × expression value of LOX) + (0.087153 × expression value of HEYL) + (0.017439 × expression value of VCAN) + (0.288547 × expression value of IGFBP7) + (−0.741817 × expression value of TWIST2) + (0.281551 × expression value of ATP1B2). The constructed prognostic model achieved a concordance index (C-index) of 0.7019, indicating that the model had good discrimination ability.[34]

Additionally, ROC curve analysis was performed to assess the predictive performance of the prognostic model. As shown in Figure 2E, the AUC values for 2-, 3-, and 5-year survival in the TCGA training cohort were 0.736, 0.728, and 0.799, respectively. Furthermore, the AUC values of the test set and the GSE84437 validation set also demonstrated good predictive performance (Figure 2F and G). The KM analysis showed significant differences in survival rates among different risk groups (Figure 2H–J).

Construction and Validation of a Prognostic Nomogram for GC Survival

Multivariate Cox regression analysis identified N stage and risk score as significant independent prognostic factors for GC patients (Figure 3A). Based on these factors, a nomogram model was built to predict survival probabilities

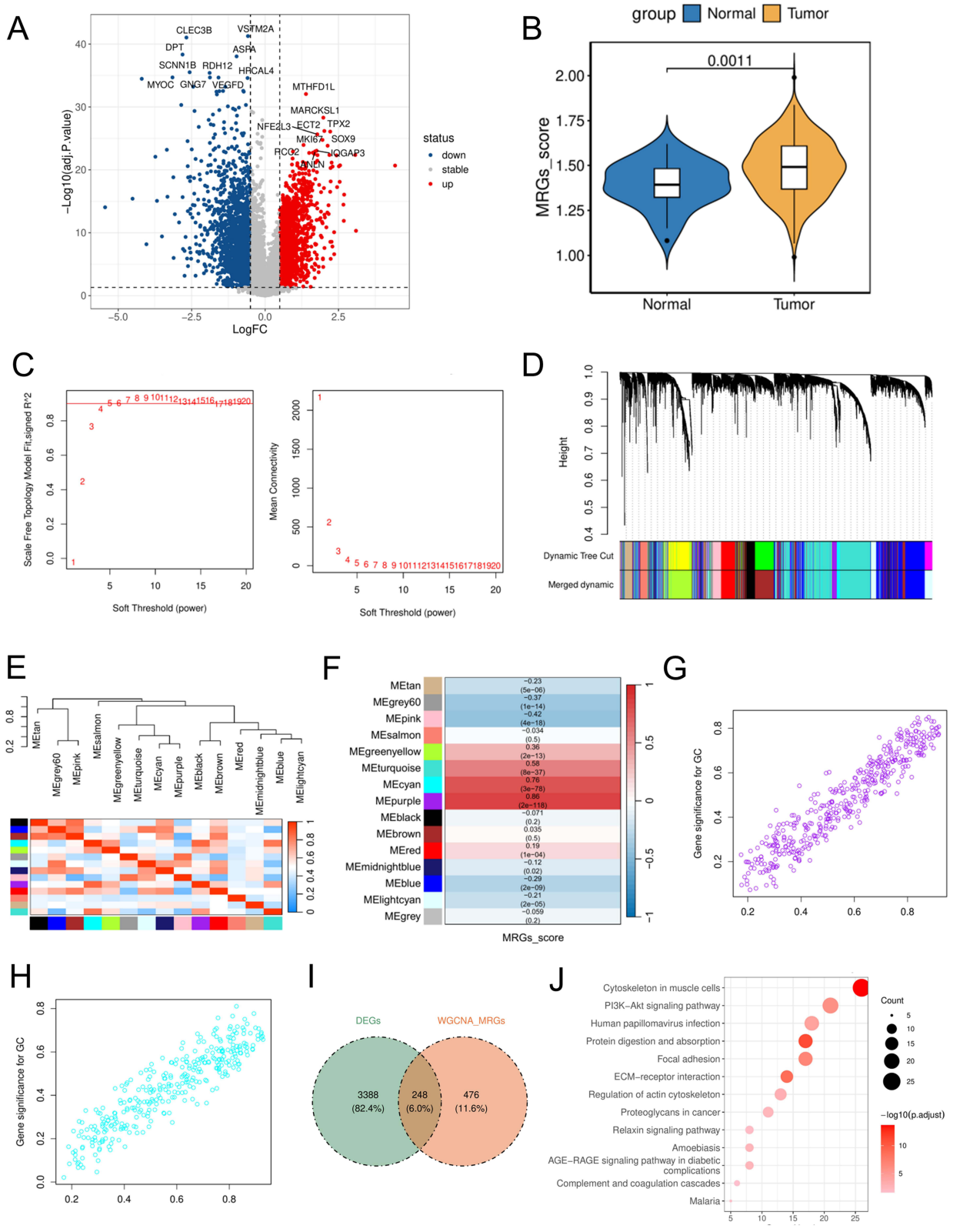

Figure 1 Identification and functional analysis of tumor mechanics-related genes in GC. (**A**) Volcano plot of DEGs between GC tissues and normal tissues. (**B**) Violin plot displaying the distribution of MRG scores calculated via ssGSEA. (**C**) Determination of the optimal soft threshold power for network construction using the WGCNA algorithm. (**D**) The variance is in the top 50% of the gene cluster dendrogram, branches represent individual genes and colors indicate distinct co-expression modules. (**E**) Clustering heatmap of gene modules. (**F**) Heatmap of module-trait relationships showing correlation coefficients and p-values; the red module exhibits the strongest correlation with MRG scores. (**G** and **H**) Scatter plots showing the strong correlations between gene significance and module membership in the purple (**G**) and cyan (**H**) modules. Specifically, the purple module exhibited an exceptionally high correlation (cor=0.95, p<1e-200), while the cyan module also showed a robust correlation (cor=0.91, p=1.1e-126). (**I**) The overlap between DEGs and mechanics-related genes. (**J**) KEGG enrichment analysis of 248 genes.

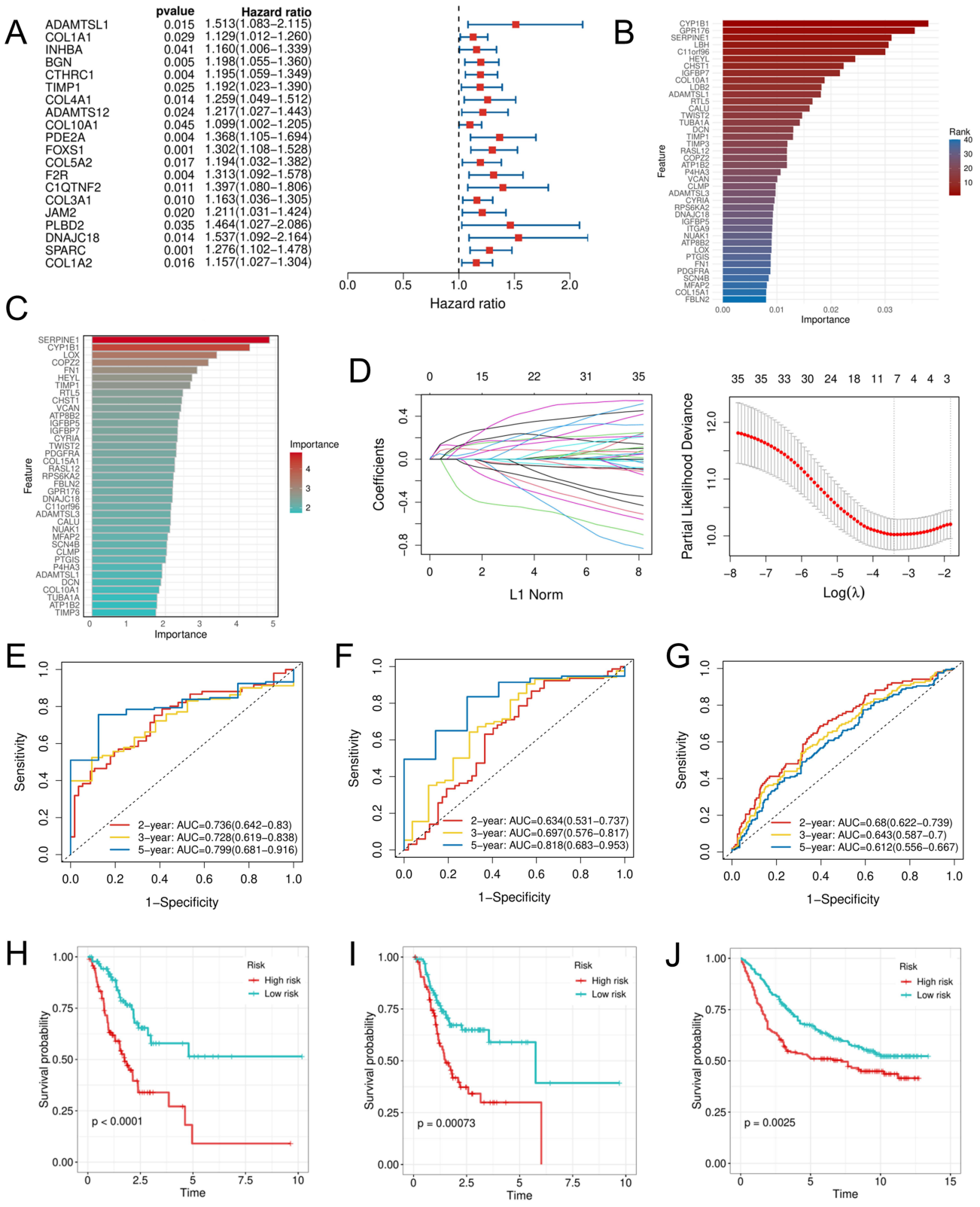

Figure 2 Machine learning-based screening of prognostic genes and risk model construction in GC. (**A**) Forest plot of univariate Cox regression analysis. (**B**) Top 40 genes selected by the XGBoost algorithm. (**C**) 37 genes selected by the SVM algorithm. (**D**) Feature selection using LASSO regression. (**E–G**) ROC curves for predicting 2-, 3-, and 5-year survival in the training set (**E**), test set (**F**), and external validation set (**G**), note the lower AUCs in the external validation cohort compared with the training and test sets. (**H–J**) Kaplan–Meier survival curves for risk groups in the training set (**H**), test set (**I**), and external validation set (**J**).

https://doi.org/10.2147/IJGM.S557444

Table 2 Multivariate Cox Regression Analysis of Prognostic Genes

Gene	Coefficients	HR	L95CI	H95CIH
SERPINE1	0.494995	1.640489	1.155694	2.328649
CYP1B1	0.154756	1.167374	0.806461	1.689804
LOX	0.298706	1.348114	0.877509	2.071103
HEYL	0.087153	1.091064	0.700522	1.699333
VCAN	0.017439	1.017592	0.653423	1.584721
IGFBP7	0.288547	1.334486	0.873422	2.038940
TWIST2	−0.741817	0.476248	0.307327	0.738014
ATP1B2	0.281551	1.325183	0.917363	1.914303

(Figure 3B). The resulting model demonstrated good discriminative performance, achieving a concordance index (C-index) of 0.7166. The predictive validity of this index was reliably confirmed by calibration curve verification (Figure 3C). Furthermore, ROC curve analysis yielded an AUC of 0.659, supporting the model's discriminative ability (Figure 3D–F). Additionally, KM survival curves revealed that elevated nomogram scores were associated with poorer survival (Figure 3G–I). Meanwhile, deceased patients were mainly distributed in the high-risk group (Figure S2A–C).

Subsequently, patients were categorized into high- and low-risk groups according to the risk scores derived from the prognostic model. Significant disparities in survival outcomes were observed between the two groups after stratification according to sex, age, T stage, N stage, and stage ($p < 0.05$) (Figure 4A–E). Moreover, integration of the risk score with clinical parameters demonstrated a strong association with tumor progression indicators, which was consistent with findings from the validation cohort (Figure 4F and G).

Differential Biological Pathways and Prognostic Genes Expression in High- vs Low-Risk GC Patients

To explore the underlying biological mechanisms, GSEA was performed on GC patients stratified into high- and low-risk groups. High-risk patients showed enrichment in GO terms related to cardiac muscle contraction, calcium-mediated signaling, and modulation of phagocytosis (Figure 5A). KEGG pathway analysis revealed significant enrichment in cell adhesion molecules, cytokine-cytokine receptor interaction, and calcium signaling pathway (Figure 5B).

To further investigate the expression patterns of 8 prognostic genes in GC and normal tissues, their expression levels were analyzed. In the TCGA dataset and external validation sets (GSE66229 and GSE54129), SERPINE1, LOX, VCAN, and IGFBP7 were significantly overexpressed in tumor tissues (Figure 5C–E). Survival analysis revealed that patients with low expression of these four genes had a significantly better survival rate than those with high expression, a finding that was further validated in the GSE84437 data set (Figure 5F). Finally, dot plots demonstrate the differential expression patterns of these genes in the 13 cancer types (Figures 5G and S3A–D).

Immune Infiltration Analysis of the Risk Score Model

To investigate the relationship between immune cells and the risk model, we applied multiple algorithms, including MCP-counter, ssGSEA, and ESTIMATE algorithm. The results revealed that ESTIMATE, immune, and stromal scores were significantly elevated in high-risk patients compared to those in the low-risk patients, and all three scores showed a positive correlation with the risk score (Figure 6A and B). In addition, the MCP-counter revealed that 10 cell types were significantly enriched in high-risk patients and showed strong positive correlations with prognostic genes, particularly dendritic cells, monocytes, fibroblasts, endothelial cells, and cytotoxic lymphocytes (Figure 6C and D). To further validate the above findings, ssGSEA was conducted to evaluate 28 types of immune cells. As expected, the high-risk group exhibited significantly elevated levels of multiple immune cells, including Tregs, macrophages, and mast cells (Figure 6E). The correlation heatmap in Figure 6F showed that SERPINE1, LOX, VCAN, and IGFBP7 were positively

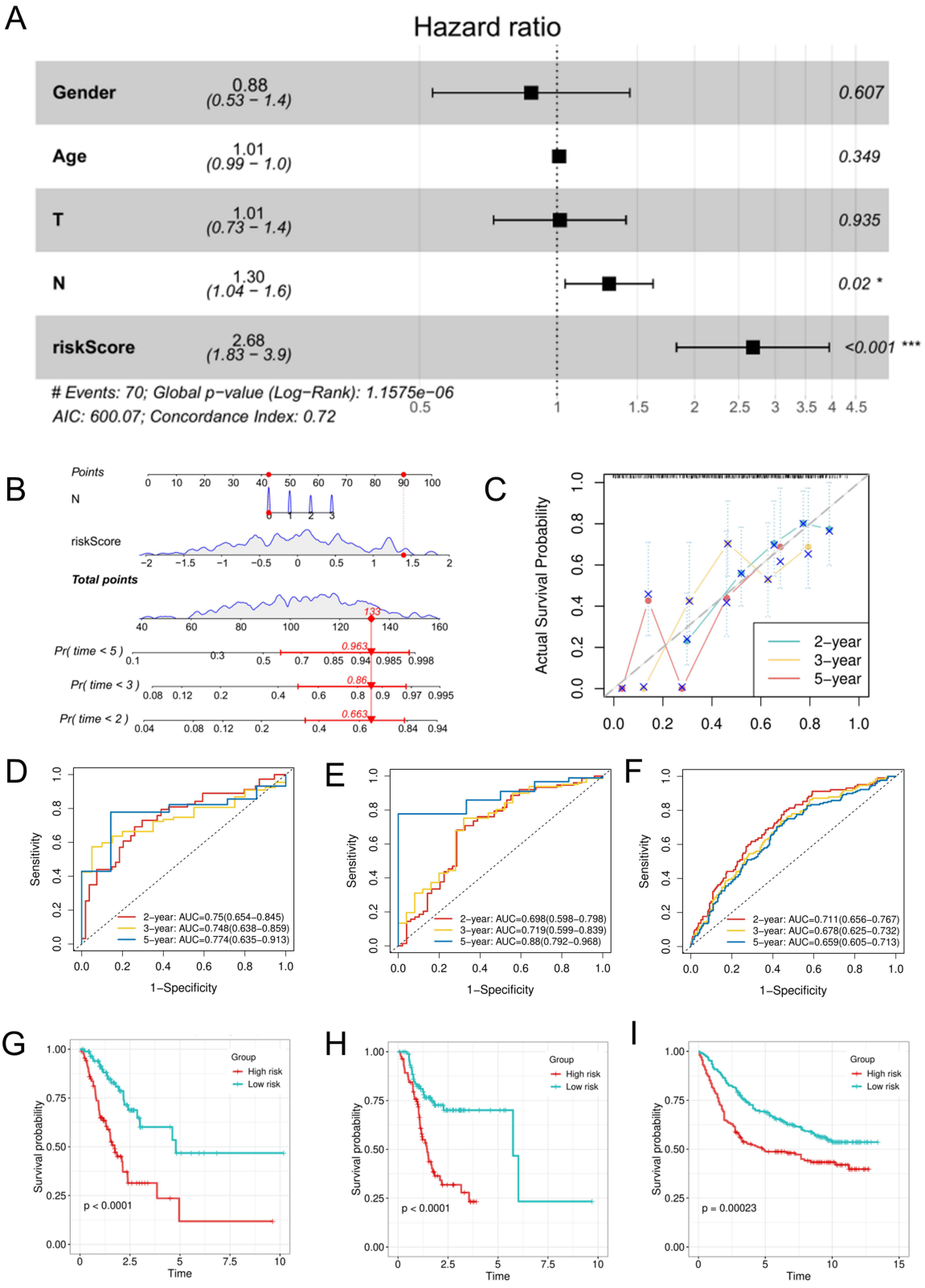

Figure 3 Construction and evaluation of the nomogram. (**A**) Multivariate Cox regression analysis. (**B**) Nomogram based on the prognostic signature consisting of risk score and clinical variables. (**C**) Calibration curves of actual survival at 2-, 3- and 5-years in the nomogram. (**D-F**) ROC curve illustrating the predictive performance of the risk model in the training set (**D**), test set (**E**), and external validation set GSE84437 (**F**). (**G-I**) Kaplan–Meier survival curves for high- and low-risk groups in the training set (**G**), test set (**H**), and GSE84437 validation cohort (**I**). ****p < 0.0001. ***p < 0.01, *p < 0.05.

https://doi.org/10.2147/IJGM.S557444

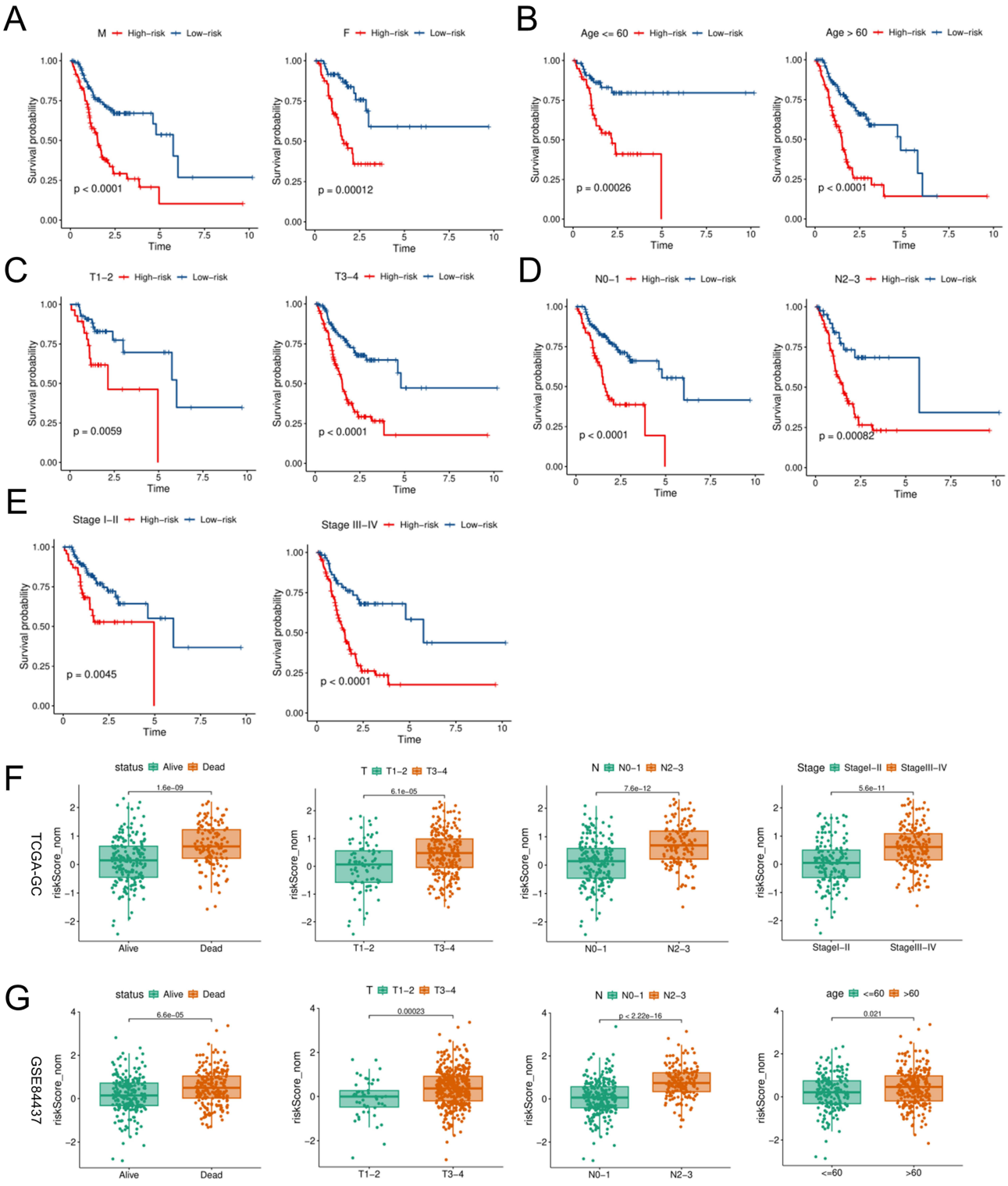

Figure 4 Analysis of clinical characteristics of GC patients in the risk score model. (**A–E**) Kaplan-Meier survival curves for high- and low-risk groups stratified by clinical characteristics in the TCGA cohort: (**A**) Sex (Male, Female), (**B**) Age (≤60, >60), (**C**) T stage (T1-2, T3-4), (**D**) N stage (N0-1, N2-3), (**E**) Stage (Stage I–II, Stage III–IV). (**F**) Correlation between risk score and clinical indicators in the TCGA-GC cohort. (**G**) Correlation between risk score and clinical indicators in the GSE84437 dataset.

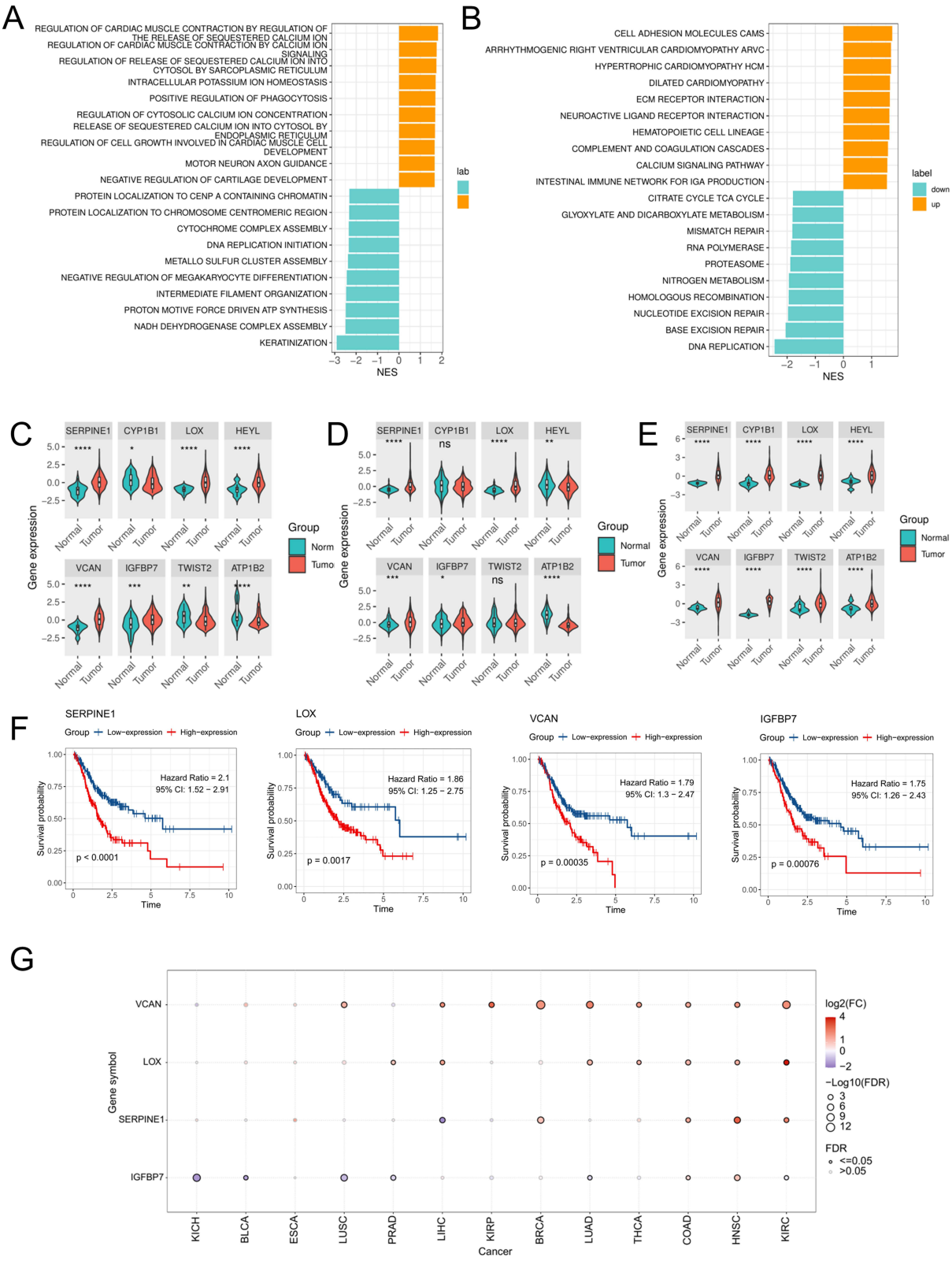

Figure 5 Differential biological pathways and prognostic genes expression in high- vs Low-risk GC patients. (**A**) GO analysis of different risk groups. (**B**) KEGG analysis of different risk groups. (**C**) Expression levels of prognostic genes in the TCGA-GC cohort. (**D**) Expression levels of prognostic genes in the GSE66229 cohort. (**E**) Expression levels of prognostic genes in the GSE54129 cohort. (**F**) Survival analysis of prognostic genes. (**G**) Expression of prognostic genes in 13 cancers. ****p < 0.0001, ***p < 0.001, **p < 0.01, *p < 0.05, ns stands for non-significance.

https://doi.org/10.2147/IJGM.S557444

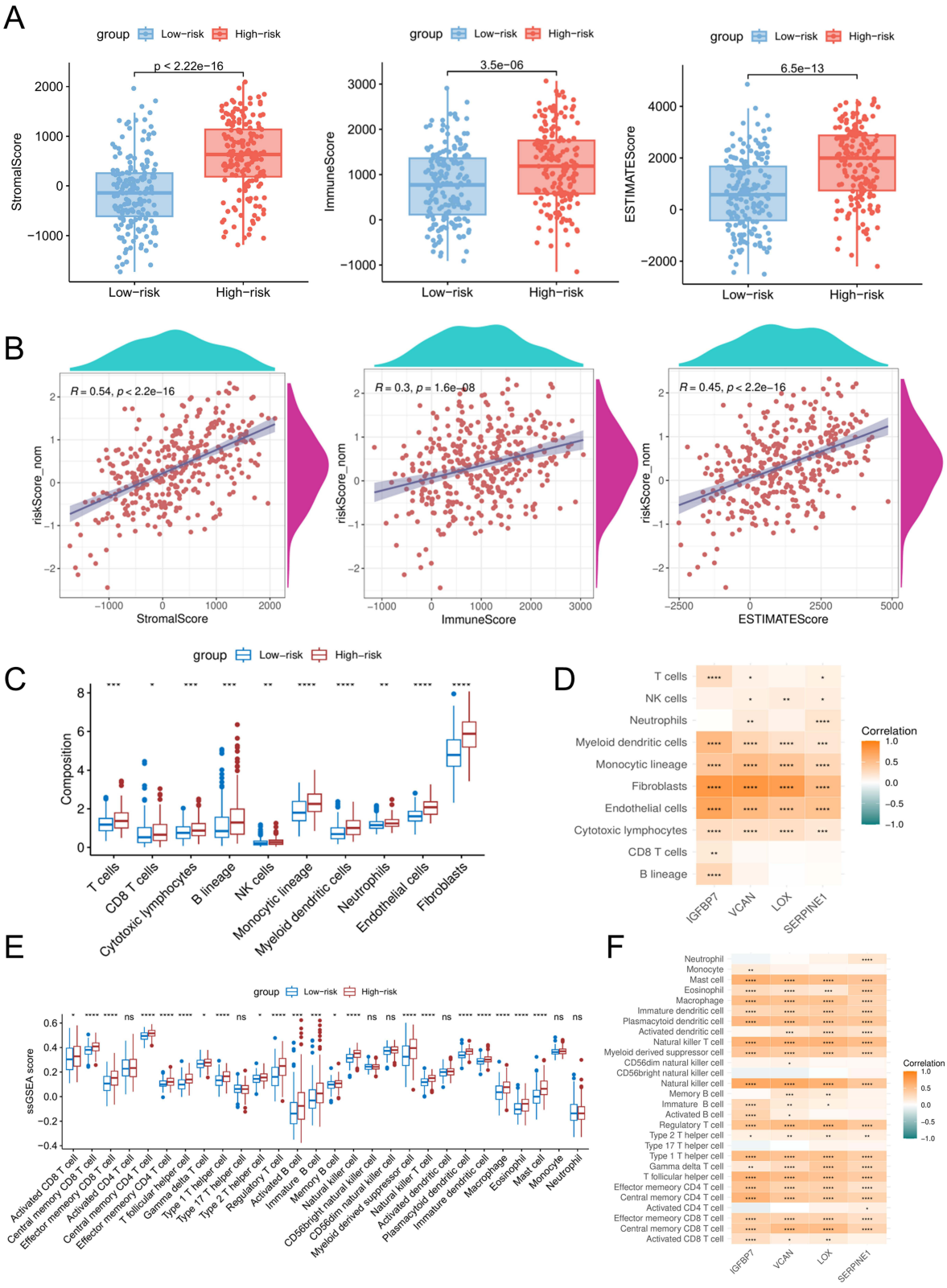

Figure 6 Function enrichment analysis and immune infiltration analysis. (**A**) Distribution of Stromal, Immune, and ESTIMATE scores across different risk groups. (**B**) Correlation between Stromal, Immune, ESTIMATE scores and risk score. (**C**) Distribution of immune cell populations in high- and low-risk samples estimated using the MCP-counter algorithm. (**D**) Heatmap showing the correlations between prognostic genes and immune cell populations calculated using the MCP-counter algorithm. (**E**) Immune cell distribution in high- and low-risk samples based on ssGSEA. (**F**) Heatmap of the correlation between genes and immune cells (ssGSEA). ****p< 0.0001, ***p< 0.001, **p< 0.01, *p< 0.05, ns stands for non-significance.

correlated with macrophages, mast cells, T cells, and other immune cells. These findings suggest that the high-risk group exhibited increased immune infiltration with immunosuppressive characteristics compared to the low-risk group.

Risk Stratification Reveals Distinct Immune Profiles, Drug Sensitivity, and ceRNA Networks in GC

To elucidate the variations in anti-cancer immune cycle steps across different risk groups, we assessed the immune activity scores in patients with GC. The results showed that release of cancer cell antigens, T cell recruitment, macrophage recruitment, and immune cell infiltration within tumor tissues were significantly enriched in high-risk patients, suggesting a more active immune response and enhanced immune cell infiltration in this group (Figure 7A). The immunophenotypic score (IPS) analysis demonstrated that patients in the low-risk group exhibited higher IPS values compared to those in the high-risk group, suggesting a potentially better response to immunotherapy (Figure 7B). In addition, both TTN and TP53 mutations were frequently observed in the two groups, with tumor mutation burden (TMB) rates exceeding 50% in each group (Figure 7C and D).

Next, we evaluated the association between patients' risk scores and their clinical responses to chemotherapy and targeted therapy for GC. The analysis revealed that the IC50 values for ABT-263, GDC-0449, Pyrimethamine, and VX-702 were significantly higher in samples from patients in the low-risk group than in samples from patients in the high-risk group. Interestingly, the low-risk group exhibited significantly greater sensitivity to Bexarotene, Epothilone B, FTI-277, Lapatinib, LFM-A13, and RO-3306 compared to the high-risk group (Figure 7E and Table S2). These results suggest that risk stratification may have predictive value for chemosensitivity and targeted therapy response.

To identify potential regulatory axes involved in GC progression, we performed a ceRNA regulatory analysis. A total of 4 miRNAs were identified through the integration of three databases (Figure 7F). Subsequently, lncRNAs targeting these miRNAs were predicted using the StarBase database, and a comprehensive lncRNA-miRNA-mRNA regulatory network was constructed based on these interactions. The resulting ceRNA network revealed that 4 specific miRNAs interacted with 16 lncRNAs and 2 mRNAs (Figure 7G).

RT-PCR Validation of Prognostic Genes

To further validate the mRNA expression levels of the identified prognostic genes, we collected six pairs of GC tissues and matched adjacent normal tissues to perform RT-PCR (Table S3). As shown in Figure 8, the expression levels of HEYL, IGFBP7, LOX, and VCAN were significantly upregulated in GC tissues, consistent with the data from TCGA. Similarly, TWIST2, ATP1B2, and CYP1B1 exhibited downregulated expression in GC tissues, aligning with their expression patterns in the TCGA dataset. These results support the robustness of our bioinformatic predictions. However, SERPINE1 was found to be downregulated in GC tissues in our RT-PCR results, which was contrary to its expression trend observed in TCGA.

Discussion

GC, one of the most frequent digestive system cancers, is strongly influenced by the formation and progression of the TME.[35,36] However, the role of tumor mechanics-related genes in GC remains unclear. Therefore, in this study, we employed bioinformatic approaches to systematically investigate the potential functions of tumor mechanics-related genes in the context of GC. In recent years, immune, ferroptosis, and metabolism-related GC prognostic models have been proposed to predict patient survival and describe the tumor microenvironment.[37–39] In contrast to these models, our prognostic model focuses on tumor mechanics-related features, including genes involved in extracellular matrix organization, tissue stiffness, and mechanical signaling, thereby capturing the often overlooked mechanical dimension of the tumor microenvironment. In addition, we combined risk scores and clinical indicators to develop a nomogram model for predicting individual outcomes in GC patients.

Initially, we obtained datasets related to GC and employed bioinformatics techniques to identify 248 tumor mechanics-related genes. Subsequently, 8 prognostic genes were identified through univariate Cox regression analysis combined with machine learning approaches. SERPINE1, a member of the serine protease inhibitor family, is associated

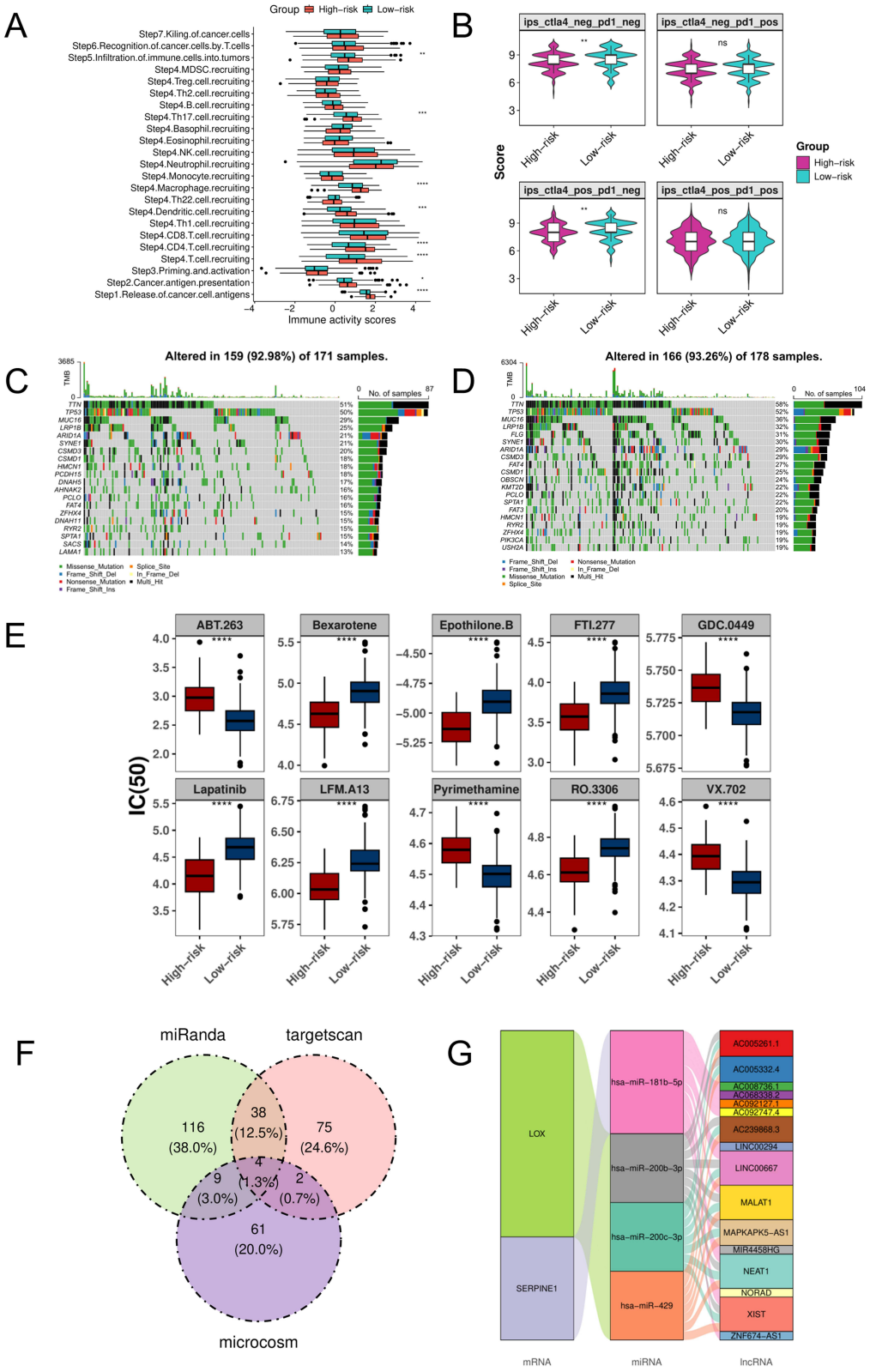

Figure 7 Risk stratification reveals distinct immune profiles, drug sensitivity, and ceRNA networks in GC. (**A**) Distribution of scores for different immune activity steps in high- and low-risk groups. (**B**) Differences in the risk score among specific tumor immunophenotypes in the TCGA-GC cohort. (**C** and **D**) Tumor somatic mutation landscapes in the high-risk (**C**) and low-risk (**D**) groups. (**E**) Drug sensitivity analysis based on GDSC-derived IC50 values for different risk groups. (**F**) Venn diagram showing predicted miRNA targets. (**G**) lncRNA-miRNA-mRNA regulatory network based on ceRNA interactions. ***p < 0.0001, ***p < 0.001, **p < 0.01, *p < 0.05, ns stands for non-significance.

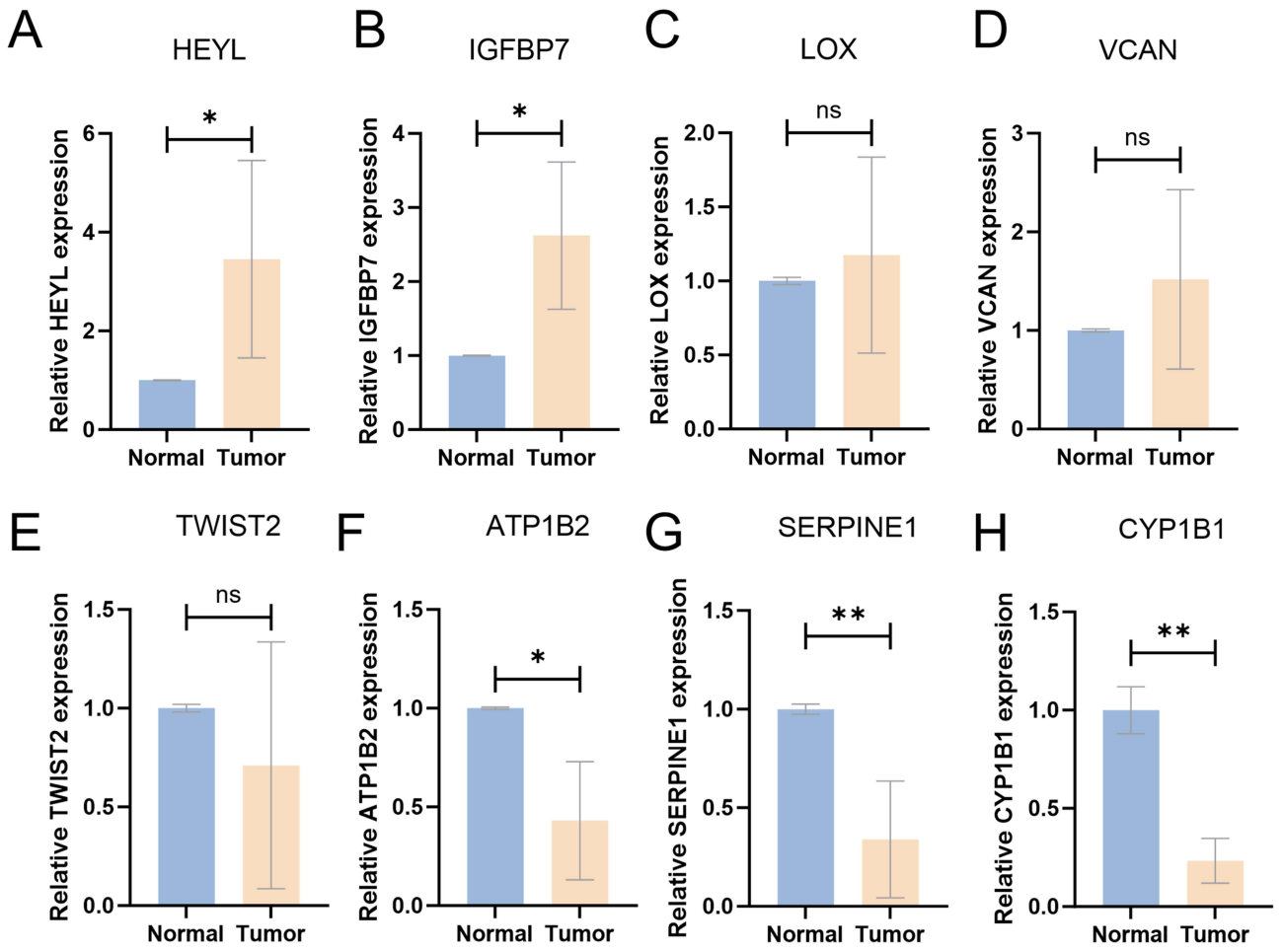

Figure 8 The RT-PCR results of HEYL (**A**), IGFBP7 (**B**), LOX (**C**), VCAN (**D**), TWIST2 (**E**), ATP1B2 (**F**), SERPINE1 (**G**), and CYP1B1 (**H**). **p < 0.01, *p < 0.05, ns stands for non-significance.

with immune responses in GC and is widely recognized for promoting tumor growth, angiogenesis, invasion, and metastasis within the tumor microenvironment.[40–42] However, SERPINE1 expression was predicted to be upregulated in GC patients by bioinformatic analyses, but RT–PCR analysis showed significantly downregulated expression. This difference may result from sample heterogeneity. The Chinese GC tissue samples collected in this study differ from those in the GEO datasets, which include patients of diverse ethnic backgrounds. Moreover, batch effects between sequencing and RT–PCR platforms, differences in tissue processing or RNA integrity, and inter-patient differences in tumor stage, grade, or anatomical location may also have contributed to this discrepancy. Finally, the small size of our validation cohort (n = 6) may have affected the RT-PCR results. Therefore, it is necessary for future studies to further confirm the biological significance of SERPINE1 in gastric cancer through larger multicenter cohorts, combined with protein level detection and functional experiments. Zhu et al demonstrated that LOX is significantly upregulated in GC tissues, suggesting its potential involvement in regulating key pathways and modulating immune activity within the TME.[43] Moreover, previous studies have shown that VCAN modulates tumor mutation burden and contributes to the remodeling of the tumor microenvironment in GC, ultimately affecting patient prognosis.[44] IGFBP7 has also been identified as an independent prognostic marker in GC, playing a promotive role in cell proliferation, invasion, and migration.[45] Similarly, HEYL is not only highly expressed in GC but also serves as an independent risk factor for patient prognosis.[46] TWIST2 has been reported to promote and modulate epithelial-mesenchymal transition (EMT) in multiple cancer types, thereby influencing the initiation and progression of GC.[47] CYP1B1 has also been reported to be closely associated with GC prognosis and the immune microenvironment.[48,49] Currently, research on ATP1B2 primarily focuses

on glioma and esophageal squamous cell carcinoma. The inhibition of ATP1B2 has been shown to impede cancer cell migration, indicating its potential role in regulating tumor development and progression.[50]

GSEA analysis revealed significant differences in the calcium signaling pathway and ECM-receptor interactions between the high- and low-risk groups, and these pathways have been widely reported to correlate with the prognosis of GC. Among the genes included in our model, SERPINE1, LOX, VCAN, and IGFBP7 act as key regulators of ECM architecture and remodeling. Specifically, SERPINE1 alters ECM degradation dynamics and enhances mechanical resistance within the tumor microenvironment by inhibiting MMP2 activity.[51] As a critical enzyme involved in ECM-receptor interaction, LOX overexpression increases ECM stiffness, thereby promoting angiogenesis and accelerating gastric cancer progression.[52,53] VCAN, a large extracellular proteoglycan, participates in the regulation of cell adhesion, migration, and inflammatory infiltration, ultimately facilitating tumor development.[54] IGFBP7 has also been shown to influence the deposition of tumor-associated ECM and modulate tumor cell behavior.[55] Regarding the calcium signaling pathway, dysregulation of E-cadherin disrupts cell-cell junctions and promotes dissemination of gastric cancer cells into the lymphatic system.[56] For instance, TWIST2 facilitates tumor metastasis by downregulating E-cadherin and tight junction proteins, thereby weakening calcium-dependent intercellular adhesion.[57]

Immune infiltration analysis showed that the high-risk group had a higher degree of immune cell infiltration, especially a significant increase in Tregs, dendritic cells, and macrophages, suggesting that this group may be in a more pronounced immunosuppressive state. As the predominant immunosuppressive populations in the tumor microenvironment, Tregs and macrophages play critical roles in the progression of gastric cancer. Previous studies have demonstrated that high Treg infiltration in the gastric tumor microenvironment is generally associated with poor prognosis and resistance to immunotherapy. Tregs suppress the activity of effector T cells primarily through the secretion of immunoregulatory cytokines such as TGF-β and IL-10, thereby promoting an immunosuppressive milieu and facilitating the immune escape of gastric cancer cells.[58–60] Meanwhile, macrophages in the gastric cancer microenvironment not only increase significantly in number but also preferentially polarize toward the M2 phenotype.[61] M2-type tumor-associated macrophages further recruit Tregs by secreting IL-10, TGF-β, CCL2/CCL22, and other immunosuppressive factors, establishing an interconnected suppressive network that promotes tumor growth and angiogenesis.[62–64] In addition, Wang et al reported that dendritic cells (DCs) also serve as key regulators within the gastric cancer tumor microenvironment.[65] However, DCs in the TME are frequently functionally impaired or exhibit tolerogenic phenotypes, which not only diminish their antigen-presenting capacity but also exacerbate tumor immune evasion.[66] Additionally, the lower ESTIMATE scores of patients in the low-risk group essentially reflected the overall lower proportion of nonneoplastic components of the tumor microenvironment, including immune cells and stromal cells. For example, Xu et al found in a multi-cancer cohort study that patients with lower stromal scores generally had a more significant survival advantage.[67] Notably, the low-risk group showed higher TMB and IPS despite the lower level of overall immune infiltration. It has been reported that the increase of TMB is usually accompanied by the accumulation of more somatic non-synonymous mutations, which may generate more neoantigens. These neoantigens can be recognized by the immune system, which in turn stimulates T cell-dependent immune responses and ultimately enhances anti-tumor immunity.[68,69] At the same time, the higher IPS score also suggests that this group of patients may have greater potential sensitivity to immunotherapy such as immune checkpoint inhibitors.[70] In summary, the low-risk group presents a unique immune microenvironment feature: although the level of immune infiltration is limited, the combination of high TMB and high IPS may have a greater capacity for anti-tumor immune response, and a higher potential for immunotherapy response.

Repurposing existing drugs for the treatment of GC offers a novel therapeutic strategy, which can not only reduce the time and cost associated with drug development, but also better reflect real world drug related adverse reactions. Our analysis revealed significant differences in sensitivity to ten drugs, including lapatinib and bexarotene, between high- and low-risk groups. Lapatinib competitively binds to the ATP-binding sites in the kinase domain of EGFR and HER2, thereby effectively inhibiting the downstream targets and affecting the survival of GC cells.[71] As an RXR agonist, bexarotene can inhibit angiogenesis and prevent drug resistance by regulating RXRα and RXRβ related signaling in GC.[72,73] These findings suggest that the risk model may offer a novel approach for guiding personalized drug selection and optimizing treatment strategies in GC patients. The ceRNA regulatory network offers a novel entry point for exploring the potential post-transcriptional regulatory mechanisms involved in GC. Although the construction of this

network largely relies on database-based predictions, several of the implicated miRNAs have previously been reported to participate in the proliferation, metastasis, or drug resistance of gastrointestinal malignancies. These findings support the hypothesis that they may, to some extent, contribute to gastric cancer progression. For example, miR-200c is typically downregulated in GC tissues and is associated with multiple biological processes, including angiogenesis, EMT, and the TGF-β signaling pathway, collectively promoting tumor progression and metastasis.[74] As another member of the miR-200 family, miR-429 has been shown to inhibit cell proliferation when overexpressed in GC cells.[75] In addition, miR-200b-3p is significantly downregulated in most GC tissues and cell lines, and its reduced expression correlates with poor patient prognosis. It may influence tumor development by regulating cell viability, invasion, and cell-cycle progression.[76] Meanwhile, lncRNAs such as MALAT1 and NEAT1 can bind to miR-200b-3p through a sponge-like adsorption mechanism, thereby regulating the expression of downstream genes and participating in tumor progression by activating EMT pathways.[77–79] It should be noted, however, that most of these lncRNA-miRNA-mRNA regulatory axes are still supported primarily by predictive analyses or indirect evidence, and their precise biological roles require further experimental validation.

This study identified 8 tumor mechanics-related prognostic biomarkers through comprehensive bioinformatics analyses and preliminary experimental validation. Several limitations should be noted. Methodologically, WGCNA was performed on the entire transcriptome, whereas ssGSEA-derived MRG scores were used solely as external phenotypic traits to identify co-expression modules associated with mechanics-related biological variation. While this approach enables the detection of broader transcriptomic patterns, using a trait derived from a subset of genes may introduce a degree of dependence. In addition, the reliability and robustness of the bioinformatics results may be influenced by the quality and completeness of the original datasets. Although RT-PCR provided preliminary validation, the number of clinical samples was limited, potentially constraining the generalizability of the findings. Future studies will involve expanding the clinical cohort to strengthen validation. Moreover, comprehensive in vitro and in vivo experiments are needed to elucidate the mechanistic roles of these biomarkers in GC progression and to further evaluate their translational potential.

Conclusion

In conclusion, this study identified eight mechanics-related prognostic genes in GC through the integration of multiple machine-learning approaches and constructed a prognostic model based on these features. Although the model exhibited favorable predictive performance in the training dataset and moderate performance in external validation datasets, further verification is still needed. These findings provide preliminary insights into the tumor mechanics underlying GC prognosis. However, additional validation in larger, multicenter cohorts and experimental studies is warranted to confirm the clinical utility of this model.

Abbreviations

GC, Gastric Cancer; TCGA, The Cancer Genome Atlas; GEO, Gene Expression Omnibus; DEGs, Differentially expressed genes; WGCNA, Weighted gene co-expression network analysis; MRGs, Mechanics-related genes; WGCNA-MRGs, Key MRG-related modules; T-MRGs, Tumor mechanistic-related genes; IPS, Immunophenotypic score; TMB, Tumor mutation burden; TME, Tumor microenvironment; ECM, Extracellular matrix; ssGSEA, Single-sample gene set enrichment analysis; TOM, Topological overlap matrix; GO, Gene Ontology; KEGG, Kyoto Encyclopedia of Genes and Genomes; ROC, Receiver operating characteristic; K-M, Kaplan-Meier; GSCA, Gene Set Cancer Analysis; GSEA, Gene Set Enrichment Analysis; MSigDB, Molecular Signatures Database; TIP, Tracking Tumor Immunophenotype; TCIA, The Cancer Immunome Atlas; ceRNA, Competing endogenous RNA; GDSC, Genomics of Drug Sensitivity in Cancer; Tregs, Regulatory T cells; DCs, Dendritic cells; FDR, False discovery rate.

Data Sharing Statement

All data used in this study were described in the main text.

Ethics Approval and Consent to Participate

This study was conducted in accordance with the Declaration of Helsinki and was approved by the Ethics Committee of The First Affiliated Hospital of Anhui Medical University (approval number: PJ-YX2025-043) on July 1, 2025. Consent to participate in the study was obtained from all participating subjects.

Acknowledgments

We are grateful to the TCGA and GEO databases for providing data support for this study. We would also like to thank the participants who participated in this study.

Author Contributions

All authors made a significant contribution to the work reported. MZ conceived the study, designed the research framework, performed data acquisition, conducted bioinformatic analyses, and drafted the initial manuscript. QL contributed to the study design, collected tissue samples, assisted with experimental execution, and participated in data interpretation. AM contributed to critical revision of the manuscript, provided analytical suggestions, and supported the interpretation of results. All authors took part in drafting, revising, or critically reviewing the article; gave final approval of the version to be published; agreed on the journal to which the article has been submitted; and agreed to be accountable for all aspects of the work.

Funding

The work was supported by the Clinical Science Foundation project of Anhui Medical University (2023xkj169) and the Scientific research project of colleges and universities in Anhui Province (2023AH050668).

Disclosure

The authors declare no conflicts of interest.

References

1. Li X, Wang X, Yu F, et al. Development and validation of a prognostic and drug sensitivity model for gastric cancer utilizing telomere-related genes. *Transl Oncol*. 2025;52:102232. doi:10.1016/j.tranon.2024.102232
2. Skubleny D, Purich K, McLean DR, et al. The tumor immune microenvironment drives survival outcomes and therapeutic response in an integrated molecular analysis of gastric adenocarcinoma. *Clin Cancer Res*. 2024;30(23):5385–5398. doi:10.1158/1078-0432.CCR-23-3523
3. Booth ME, Wood HM, Travis MA, et al. The relationship between the gastric cancer microbiome and clinicopathological factors: a metagenomic investigation from the 100,000 genomes project and the cancer genome atlas. *Gastric Cancer*. 2025;28(3):358–371. doi:10.1007/s10120-025-01588-9
4. Zeng Y, Jin RU. Molecular pathogenesis, targeted therapies, and future perspectives for gastric cancer. *Semin Cancer Biol*. 2022;86(Pt 3):566–582. doi:10.1016/j.semcancer.2021.12.004
5. GBD 2019 Cancer Risk Factors Collaborators. The global burden of cancer attributable to risk factors, 2010-19: a systematic analysis for the global burden of disease study 2019. *Lancet*. 2022;400(10352):563–591. doi:10.1016/S0140-6736(22)01438-6
6. Filli L, Rosskopf AB, Sutter R, et al. MRI predictors of posterolateral corner instability: a decision tree analysis of patients with acute anterior cruciate ligament tear. *Radiology*. 2018;289(1):170–180. doi:10.1148/radiol.2018180194
7. Eum HH, Kwon M, Ryu D, et al. Tumor-promoting macrophages prevail in malignant ascites of advanced gastric cancer. *Exp Mol Med*. 2020;52(12):1976–1988. doi:10.1038/s12276-020-00538-y
8. Li X, Sun Z, Peng G, et al. Single-cell RNA sequencing reveals a pro-invasive cancer-associated fibroblast subgroup associated with poor clinical outcomes in patients with gastric cancer. *Theranostics*. 2022;12(2):620–638. doi:10.7150/thno.60540
9. Ren L, Huang D, Liu H, et al. Applications of single-cell omics and spatial transcriptomics technologies in gastric cancer (Review). *Oncol Lett*. 2024;27(4):152. doi:10.3892/ol.2024.14285
10. Li Z, Xie Q, Zhao F, et al. Exploring GZMK as a prognostic marker and predictor of immunotherapy response in breast cancer: unveiling novel insights into treatment outcomes. *J Cancer Res Clin Oncol*. 2024;150(6):286. doi:10.1007/s00432-024-05791-6
11. Mansour RM, El-Sayyad GS, Abulsoud AI, et al. The role of miRNAs in pathogenesis, diagnosis, and therapy of Helicobacter pylori infection, gastric cancer-causing bacteria: special highlights on nanotechnology-based therapy. *Microb Pathog*. 2025;205:107646. doi:10.1016/j.micpath.2025.107646
12. Nia HT, Liu H, Seano G, et al. Solid stress and elastic energy as measures of tumour mechanopathology. *Nat Biomed Eng*. 2016;1(1):0004. doi:10.1038/s41551-016-0004
13. Nia HT, Munn LL, Jain RK. Physical traits of cancer. *Science*. 2020;370(6516):eaaz0868. doi:10.1126/science.aaz0868
14. Samuel MS, Lopez JI, McGhee EJ, et al. Actomyosin-mediated cellular tension drives increased tissue stiffness and β-catenin activation to induce epidermal hyperplasia and tumor growth. *Cancer Cell*. 2024;42(2):317. doi:10.1016/j.ccell.2023.12.014

15. Kümper S, Marshall CJ. ROCK-driven actomyosin contractility induces tissue stiffness and tumor growth. *Cancer Cell*. 2011;19(6):695–697. doi:10.1016/j.ccr.2011.05.021
16. Xin Y, Li K, Huang M, et al. Biophysics in tumor growth and progression: from single mechano-sensitive molecules to mechanomedicine. *Oncogene*. 2023;42(47):3457–3490. doi:10.1038/s41388-023-02844-x
17. Liu Y, Xu YQ, Long YY, et al. Mechanosensitive channel Piezo1 in calcium dynamics: structure, function, and emerging therapeutic strategies. *Front Mol Biosci*. 2025;12:1693456. doi:10.3389/fmolb.2025.1693456
18. Shakiba D, Genin GM, Zustiak SP. Mechanobiology of cancer cell responsiveness to chemotherapy and immunotherapy: mechanistic insights and biomaterial platforms. *Adv Drug Deliv Rev*. 2023;196:114771. doi:10.1016/j.addr.2023.114771
19. Luo X, Hong L, Cheng C, et al. DNMT1 mediates metabolic reprogramming induced by Epstein-Barr virus latent membrane protein 1 and reversed by grifolin in nasopharyngeal carcinoma. *Cell Death Dis*. 2018;9(6):619. doi:10.1038/s41419-018-0662-2
20. Zhao F, Zhang L, Wei M, et al. Mechanosensitive ion channel PIEZO1 signaling in the hall-marks of cancer: structure and functions. *Cancers*. 2022;14(19):4955. doi:10.3390/cancers14194955
21. Zhang P, Li P, Tang M, et al. The genomic and immunogenomic landscape of mechanics pathway informs clinical prognosis and response to mechanotherapy. *Sci China Life Sci*. 2024;67(8):1549–1562. doi:10.1007/s11427-024-2622-1
22. Sun Z, Jing C, Xiao C, et al. Long non-coding RNA profile study identifies an immune-related lncRNA prognostic signature for kidney renal clear cell carcinoma. *Front Oncol*. 2020;10:1430. doi:10.3389/fonc.2020.01430
23. He YB, Fang LW, Hu D, et al. Necroptosis-associated long noncoding RNAs can predict prognosis and differentiate between cold and hot tumors in ovarian cancer. *Front Oncol*. 2022;12:967207. doi:10.3389/fonc.2022.967207
24. Barbie DA, Tamayo P, Boehm JS, et al. Systematic RNA interference reveals that oncogenic KRAS-driven cancers require TBK1. *Nature*. 2009;462(7269):108–112. doi:10.1038/nature08460
25. Thomas PD, Ebert D, Muruganujan A, et al. PANTHER: making genome-scale phylogenetics accessible to all. *Protein Sci*. 2022;31(1):8–22. doi:10.1002/pro.4218
26. Kanehisa M, Furumichi M, Sato Y, et al. KEGG: biological systems database as a model of the real world. *Nucleic Acids Res*. 2025;53(D1):D672–D677. doi:10.1093/nar/gkae909
27. Szklarczyk D, Kirsch R, Koutrouli M, et al. The STRING database in 2023: protein-protein association networks and functional enrichment analyses for any sequenced genome of interest. *Nucleic Acids Res*. 2023;51(D1):D638–D646. doi:10.1093/nar/gkac1000
28. Liu CJ, Hu FF, Xie GY, et al. GSCA: an integrated platform for gene set cancer analysis at genomic, pharmacogenomic and immunogenomic levels. *Brief Bioinform*. 2023;24(1):bbac558. doi:10.1093/bib/bbac558
29. Subramanian A, Tamayo P, Mootha VK, et al. Gene set enrichment analysis: a knowledge-based approach for interpreting genome-wide expression profiles. *Proc Natl Acad Sci U S A*. 2005;102(43):15545–15550. doi:10.1073/pnas.0506580102
30. Castanza AS, Recla JM, Eby D, et al. Extending support for mouse data in the Molecular Signatures Database (MSigDB). *Nat Methods*. 2023;20 (11):1619–1620. doi:10.1038/s41592-023-02014-7
31. Yoshihara K, Shahmoradgoli M, Martínez E, et al. Inferring tumour purity and stromal and immune cell admixture from expression data. *Nat Commun*. 2013;4:2612. doi:10.1038/ncomms3612
32. Becht E, Giraldo NA, Lacroix L, et al. Estimating the population abundance of tissue-infiltrating immune and stromal cell populations using gene expression. *Genome Biol*. 2016;17(1):218. doi:10.1186/s13059-016-1070-5
33. Xu L, Deng C, Pang B, et al. TIP: a web server for resolving tumor immunophenotype profiling. *Cancer Res*. 2018;78(23):6575–6580. doi:10.1158/0008-5472.CAN-18-0689
34. Guo Z, Zhou H, Lv D, et al. Tumor necrosis-informed prognostic nomogram for clear cell renal cell carcinoma model development and clinical validation. *BMC Urol*. 2025;25(1):252. doi:10.1186/s12894-025-01940-2
35. He L, Qian X, Ge P, et al. NOL6 regulates the proliferation and apoptosis of gastric cancer cells via regulating TP53I3, CDK4 and MCM7 expression. *Front Oncol*. 2022;12:708081. doi:10.3389/fonc.2022.708081
36. Xie J, Zheng S, Zou Y, et al. Turning up a new pattern: identification of cancer-associated fibroblast-related clusters in TNBC. *Front Immunol*. 2022;13:1022147. doi:10.3389/fimmu.2022.1022147
37. Wang H, Chen H, Liu J, et al. Identification of key ferroptosis-related genes associated with the development of gastric cancer: prognostic models, molecular mechanisms and potential treatment strategies. *Oncol Lett*. 2025;30(4):450. doi:10.3892/ol.2025.15196
38. Liu Y, Li D, Chen Y, et al. Integrated bioinformatics analysis for conducting a prognostic model and identifying immunotherapeutic targets in gastric cancer. *BMC Bioinf*. 2023;24(1):191. doi:10.1186/s12859-023-05312-1
39. Shao Y, Chen C, Yu X, et al. Comprehensive analysis of scRNA-seq and bulk RNA-seq data via machine learning and bioinformatics reveals the role of lysine metabolism-related genes in gastric carcinogenesis. *BMC Cancer*. 2025;25(1):644. doi:10.1186/s12885-025-14051-w
40. Zhang H, Zhang Y, Li Y, et al. Bioinformatics and network pharmacology identify the therapeutic role and potential mechanism of melatonin in AD and rosacea. *Front Immunol*. 2021;12:756550. doi:10.3389/fimmu.2021.756550
41. Sabol RA, Beighley A, Giacomelli P, et al. Obesity-altered adipose stem cells promote ER+ breast cancer metastasis through estrogen independent pathways. *Int J Mol Sci*. 2019;20(6):1419. doi:10.3390/ijms20061419
42. Yuan Y, Zhou D, Chen F, et al. SIX5-activated LINC01468 promotes lung adenocarcinoma progression by recruiting SERBP1 to regulate SERPINE1 mRNA stability and recruiting USP5 to facilitate PAI1 protein deubiquitylation. *Cell Death Dis*. 2022;13(4):312. doi:10.1038/s41419-022-04717-9
43. Zhu J, Luo C, Zhao J, et al. Expression of LOX suggests poor prognosis in gastric cancer. *Front Med*. 2021;8:718986. doi:10.3389/fmed.2021.718986
44. Song J, Wei R, Huo S, et al. Versican enrichment predicts poor prognosis and response to adjuvant therapy and immunotherapy in gastric cancer. *Front Immunol*. 2022;13:960570. doi:10.3389/fimmu.2022.960570
45. Tomić TT, Olausson J, Rehammar A, et al. MYO5B mutations in pheochromocytoma/paraganglioma promote cancer progression. *PLoS Genet*. 2020;16(6):e1008803. doi:10.1371/journal.pgen.1008803
46. Zhou L, Lu H, Zeng F, et al. Constructing a new prognostic signature of gastric cancer based on multiple data sets. *Bioengineered*. 2021;12 (1):2820–2835. doi:10.1080/21655979.2021.1940030

47. Tan YE, Xing Y, Ran BL, et al. LINC01235-TWIST2 feedback loop facilitates epithelial-mesenchymal transition in gastric cancer by inhibiting THBS2. *Aging*. 2020;12(24):25060–25075. doi:10.18632/aging.103979
48. Zhang L, Hu D, Huangfu S, et al. DNA repair and replication-related gene signature based on tumor mutation burden reveals prognostic and immunotherapy response in gastric cancer. *J Oncol*. 2022;2022:6469523. doi:10.1155/2022/6469523
49. Lv JW, Zheng ZQ, Wang ZX, et al. Pan-cancer genomic analyses reveal prognostic and immunogenic features of the tumor melatonergic microenvironment across 14 solid cancer types. *J Pineal Res*. 2019;66(3):e12557. doi:10.1111/jpi.12557
50. Liu FF, Wen H, Liu XB, et al. Overexpression of ATP1B2 promotes cancer cell migration and inhibits apoptosis in patients with esophageal squamous cell carcinoma. *Oncol Rep*. 2025;54(2):96. doi:10.3892/or.2025.8929
51. Zaheer J, Shanmugiah J, Kim S, et al. Tumor microenvironment modulation by SERPINE1 increases radioimmunotherapy in murine model of gastric cancer. *Sci Rep*. 2025;15(1):16449. doi:10.1038/s41598-025-97983-4
52. Farhat A, Ferns GA, Ashrafi K, et al. Lysyl oxidase mechanisms to mediate gastrointestinal cancer progression. *Gastrointest Tumors*. 2021;8(1):33–40. doi:10.1159/000511244
53. Qiu Z, Jiang H, Ju K, et al. A novel RNA-binding protein signature to predict clinical outcomes and guide clinical therapy in gastric cancer. *Front Med*. 2021;8:670141. doi:10.3389/fmed.2021.670141
54. Dai R, Hua W, Chen W, et al. Isolation, characterization, and safety evaluation of human skin-derived precursors from an adherent monolayer culture system. *Stem Cells Int*. 2019;2019:9194560. doi:10.1155/2019/9194560
55. Lit KK, Zhirenova Z, Blocki A. Insulin-like growth factor-binding protein 7 (IGFBP7): a microenvironment-dependent regulator of angiogenesis and vascular remodeling. *Front Cell Dev Biol*. 2024;12:1421438. doi:10.3389/fcell.2024.1421438
56. Cai M, Nie X, Cai F, et al. Identification and validation of calcium signaling pathway-related biomarkers in T1 and T2 lymph node metastatic gastric cancer. *Front Genet*. 2025;16:1653700. doi:10.3389/fgene.2025.1653700
57. Kyuno D, Takasawa A, Kikuchi S, et al. Role of tight junctions in the epithelial-to-mesenchymal transition of cancer cells. *Biochim Biophys Acta Biomembr*. 2021;1863(3):183503. doi:10.1016/j.bbamem.2020.183503
58. Wang S, Xu X. An immune-related gene pairs signature for predicting survival in glioblastoma. *Front Oncol*. 2021;11:564960. doi:10.3389/fonc.2021.564960
59. Yu HR, Tsai CC, Chang LS, et al. l-arginine-dependent epigenetic regulation of interleukin-10, but not transforming growth factor-β, production by neonatal regulatory T lymphocytes. *Front Immunol*. 2017;8:487. doi:10.3389/fimmu.2017.00487
60. Negura I, Pavel-Tanasa M, Danciu M. Regulatory T cells in gastric cancer: key controllers from pathogenesis to therapy. *Cancer Treat Rev*. 2023;120:102629. doi:10.1016/j.ctrv.2023.102629
61. Li C, Li C, Ma Z, et al. Regulated macrophage immune microenvironment in 3D printed scaffolds for bone tumor postoperative treatment. *Bioact Mater*. 2022;19:474–485. doi:10.1016/j.bioactmat.2022.04.028
62. Yamamoto K, Makino T, Sato E, et al. Tumor-infiltrating M2 macrophage in pretreatment biopsy sample predicts response to chemotherapy and survival in esophageal cancer. *Cancer Sci*. 2020;111(4):1103–1112. doi:10.1111/cas.14328
63. Guo W, Liu GM, Guan JY, et al. Epigenetic regulation of cutaneous T-cell lymphoma is mediated by dysregulated lncRNA MALAT1 through modulation of tumor microenvironment. *Front Oncol*. 2022;12:977266. doi:10.3389/fonc.2022.977266
64. Zhou Z, Yang Z, Wang J, et al. Research progress on tumour-associated macrophages in gastric cancer (Review). *Oncol Rep*. 2021;45(4):35. doi:10.3892/or.2021.7986
65. Wang C, Chen L, Fu D, et al. Antigen presenting cells in cancer immunity and mediation of immune checkpoint blockade. *Clin Exp Metastasis*. 2024;41(4):333–349. doi:10.1007/s10585-023-10257-z
66. Wang Y, Ding N, Qi L, et al. Immunopharmacology of gastric cancer-deciphering immune cell subset responses and nanoparticle-mediated targeting. *Front Pharmacol*. 2025;16:1611234. doi:10.3389/fphar.2025.1611234
67. Xu X, Xu Y, Hu W, et al. Stromal score is a promising index in tumor patients' outcome determination. *Heliyon*. 2023;9(11):e22432. doi:10.1016/j.heliyon.2023.e22432
68. Zhou Q, Xu Y, Shen L, et al. Identification of a novel necroptosis-related classifier to predict prognosis and guide immunotherapy in breast invasive carcinoma. *Front Oncol*. 2022;12:852365. doi:10.3389/fonc.2022.852365
69. Zhu G, Pei L, Li Y, Gou X. EP300 mutation is associated with tumor mutation burden and promotes antitumor immunity in bladder cancer patients. *Aging*. 2020;12(3):2132–2141. doi:10.18632/aging.102728
70. Guo C, Tang Y, Yang Z, et al. Hallmark-guided subtypes of hepatocellular carcinoma for the identification of immune-related gene classifiers in the prediction of prognosis, treatment efficacy, and drug candidates. *Front Immunol*. 2022;13:958161. doi:10.3389/fimmu.2022.958161
71. Fu C, Sun L, Zhou X, et al. Identification and validation of prognostic genes associated with mitochondrial nuclear genes in gastric cancer. *Clin Exp Med*. 2025;25(1):309. doi:10.1007/s10238-025-01844-3
72. Garattini SK, Basile D, De Re V, et al. The potential of retinoic acid receptors as prognostic biomarkers and therapeutic targets in gastric cancer. *Front Oncol*. 2024;14:1453934. doi:10.3389/fonc.2024.1453934
73. Qu L, Tang X. Bexarotene: a promising anticancer agent. *Cancer Chemother Pharmacol*. 2010;65(2):201–205. doi:10.1007/s00280-009-1140-4
74. Shichiri K, Oshi M, Ziazadeh D, et al. High miR-200c expression is associated with suppressed epithelial-mesenchymal transition, TGF-β signaling and better survival despite enhanced cell proliferation in gastric cancer patients. *Am J Cancer Res*. 2023;13(7):3027–3040.
75. Zhang M, Dong BB, Lu M, et al. miR-429 functions as a tumor suppressor by targeting FSCN1 in gastric cancer cells. *Onco Targets Ther*. 2016;9:1123–1133. doi:10.2147/OTT.S91879
76. Li D, Li Q. MicroRNA-200b-3p restrains gastric cancer cell proliferation, migration, and invasion via C-X-C motif chemokine ligand 12/CXC chemokine receptor 7 axis. *Bioengineered*. 2022;13(3):6509–6520. doi:10.1080/21655979.2022.2034585
77. Han N, Tian W, Yu N, et al. YAP1 is required for the angiogenesis in retinal microvascular endothelial cells via the inhibition of MALAT1-mediated miR-200b-3p in high glucose-induced diabetic retinopathy. *J Cell Physiol*. 2020;235(2):1309–1320. doi:10.1002/jcp.29047
78. Thapa R, Afzal O, Afzal M, et al. From LncRNA to metastasis: the MALAT1-EMT axis in cancer progression. *Pathol Res Pract*. 2024;253:154959. doi:10.1016/j.prp.2023.154959
79. Sun BY, Gong X, Xiong CH, et al. A science-driven method for determining morphological parameters of prosthetic hands. *Bioinspir Biomim*. 2021;16(4):10. doi:10.1088/1748-3190/abcb5e